# A Study of Bubble Trajectory and Drag Co-efficient in Water and Non-Newtonian Fluids

**N. M. S. HASSAN*, M. M. K. KHAN, AND M. G. RASUL**

College of Engineering and Built Environment
Faculty of Sciences, Engineering and Health
Central Queensland University
Rockhampton, Qld-4702
AUSTRALIA
*n.hassan@cqu.edu.au ; nmshassan@gmail.com

*Abstract:* - A new experimental set-up was used to analyze the characteristics of the bubbles rising in water and three different concentrations of xanthan gum solutions for higher Reynolds number. The bubble size, bubble rise velocity, and bubble trajectory were measured using a combination of non-intrusive-high speed photographic method and digital image processing. The results of bubble trajectory for various bubbles in water and different xanthan gum solutions are presented and discussed. In trajectory analysis, it is seen that the smaller bubbles show helical or zigzag motion and larger bubbles follow spiral motion for water. In xanthan gum solutions, small bubbles experience less horizontal motion than that in water. Larger bubbles produce more spiral motion with the increase in xanthan gum concentration. Drag coefficients for air bubbles at higher Reynolds number are reported. It is seen that the experimental drag coefficient increases with the increase in xanthan gum concentration corresponding to the same bubble volume.

*Key-words:* - Bubble trajectory, bubble volume, drag co-efficient, Reynolds number, polymer solution, non-intrusive method

## 1 Introduction

The bubble rise characterization is very important for the design of heat and mass transfer operations. Air bubbles are used in chemical, biochemical, environmental, and food process for improving the heat and mass transfer. The overall mass transfer is affected by the bubble size, pressure inside the gas phase, interaction between bubbles, rise velocity and trajectory [1].

The most significant dynamic behaviour of air bubbles are the bubble rise velocity, trajectory and the drag coefficient. After formation, a bubble quickly accelerates to its terminal velocity. The terminal velocity of an air bubble is termed as the velocity attained at steady state conditions where all applied forces are balanced. The terminal rise velocity of a single bubble rising in a liquid depends on the volume of the bubble and on the physical properties of the bubble and the liquid. The bubble rising in non-Newtonian polymer solutions also depends on the rheological properties of the liquid. The bubbles will experience a lift force if the liquid is sheared, and they move perpendicular to the velocity shear and the bubble trajectory is affected by the turbulence motions of the bubble in the liquid. This effect is being strongest for bubbles whose rise is less than the turbulence velocity scale.

When a bubble rises through a liquid, the way it travels is different from the path of solid particles either rising due to buoyancy or sinking. Solid particles do not circulate internally and tend to remain rigid; however a solid particle could have the same shape as a bubble. But a gas bubble has constant motion internally. A bubble tries to follow the path of least resistance during its motion. As a bubble rises upwards through liquid, the most resistance will be directly on top. However, if the bubble moves slightly to one side, less total resistance is experienced. It is readily observed that bubbles commence a helical, or spring shaped path as they rise in a column of liquid.

Generally, the dynamics of bubble rise are nonlinear and the degree of the nonlinearity increases with bubble size [2].

Single air bubbles rising through a liquid have been studied extensively. It has been found that when the bubbles are very small, surface tension, which is predominant over the internal force and the buoyant force, makes the bubble spherical and they tend to retain the spherical shape as long as their rising velocity, thus Reynolds number (Re) remains small. In most practical situation, all three factors, inertia effect, viscosity, and surface tension should be regarded in that the bubbles are not spherical in shape and they move in an oscillatory manner. For low-Re flows, the viscous forces are large relative to internal terms. So the viscosity forces dominate the terminal motion and terminal rise velocity increases with increased of diameter of the bubble at very low Re. At intermediate region (Re>1), bubbles are no more spherical as their size increases and terminal velocity may increase or remain constant or decrease with equivalent diameter of the bubble. In this region, surface tension and inertia forces determine the terminal rise velocity. At high Re, bubbles are spherical cap or mushroom shaped and the motion of the bubble is dominated by the inertia forces. In this region, bubble rise velocity increases with the equivalent diameter of the bubble [2].

The dynamics of the bubble characteristics in a gas-liquid system are still not totally understood. From most of the study, it was seen that a small bubble rises through water in a straight line at its terminal velocity until it finishes its journey. The paths of larger bubbles were not stable and started to zigzag and much larger bubbles followed spiral motion [3 -8]. Wu and Gharib [4] studied the bubble trajectories for spherical and ellipsoidal bubbles in clean water and they showed that the ellipsoidal bubbles exhibit a spiralling path instability, while the spherical bubbles follow a zigzagging path instability when the bubble diameter exceeded 0.15 cm. Saffman [8] observed only the zigzag motions as the bubble rises in water when the radius of the bubble was less than 1 mm but bubbles of larger radius shows either zigzag or spiral motion depending upon different factors. Feng and Leal [9] verified various possible trajectories in different shape regimes. A single bubble can pursue a zigzag path at $\mathrm{Re} \approx 600$, accompanied with vortex shedding behind the bubble. Under the same experimental conditions, Yoshida and Manasseh [10] suggested that the bubbles can also pursue spiral trajectory without vortex shedding. Shew and Pinton [11] presented that the commencement of path instability for smaller bubble size changed remarkably in the case of polymer solution and it also appeared that the split to path instability for increasing bubble size was less rapid for the polymer solution in comparison with water.

Dewsbury et al. [12] investigated the relationship between the terminal velocity and volume for larger gas bubbles in non-Newtonian power-law fluids. Tsuge and Hibino [13] reported that the trajectories of rising spherical and ellipsoidal gas bubbles at higher Re were identical. Dewsbury et al. [14] determined experimentally that the drag coefficient for a rising solid sphere in non-Newtonian pseudo plastic liquids were significantly affected by its trajectory. A new drag correlation for rising spheres in non-Newtonian power-law liquids was presented by Dewsbury et al. [15]. It described the relationship between $C_d$ and Re in creeping, transitional, turbulent and even critical flow regimes and it is valid for $0.1<\mathrm{Re}<25000$. Margaritis et al. [16] studied the drag co-efficient variation for bubbles over a wide range of Re in different non-Newtonian polysaccharide solutions and proposed a correlation which matched very well with experimental data. For the case of power-law non-Newtonian fluids, it has been shown that the drag curve for air bubbles followed Hadamard-Rybczynski model rather than Stokes model for $\mathrm{Re} < 5$ [14, 17]. On the other hand, Miyahara and Yamanaka [17] reported for the case of highly viscous non-Newtonian liquid that the drag coefficient deviated from the Hadamard –Rybczynski type equation if the Re increased. Dhole et al. [18] investigated that the drag co-efficient always increased with the increase in power law index for all values of the Re.

The standard drag curves are well established for Newtonian liquid. However, no such valid correlation of the drag coefficient of the gas bubble for non-Newtonian liquids at high Re exists. Clift et al. [19] listed a large number of correlations of drag coefficient for Newtonian liquids at a wide range of Re. On the other hand, Dewsbury et al. [12, 14], Margaritis et al. [16], Miyhara and Yamanaka [17], Chhabra [20], Karamanev [21] presented the correlations for drag coefficient of gas bubble in non-Newtonian power-law liquids concerning solid particles and spherical bubbles. However, no universal drag curve for the case of rising air bubbles in non-Newtonian Power-Law fluids have been developed yet in the available literature.

The aim of this study is to measure the bubble trajectory, and the drag on the bubble as it rises through water and different concentration xanthan gum (shear thinning) solutions and investigate the influence of various parameters namely, the bubble sizes, fluid properties on the bubble rise characteristics (trajectory, drag etc). A new set of experimental data of drag coefficient for spherical and non spherical air bubble with a wide range of Reynolds number are obtained for both water and different concentrations of xanthan gum solutions.These new experimental data are compared with the results of other analytical and experimental studies available in the literature.

## 2 Experimental Set-up and Procedure

### 2.1 Experimental test rig

The experimental apparatus is shown schematically in Figure 1. Two-test rigs were used for investigating the bubble rise characteristics in water and three different concentration of xanthan gum solution. The first rig consisted of a polycarbonate tube approximately 1.8 m in height and 125 mm in diameter. A height of 1.8 m is required to allow the bubble when it is released at the bottom of the rig to reach its terminal velocity. It contains two holes near the base. One is to facilitate the removal of the liquid contained in it and the other is to make possible the insertion of gas bubbles into the test rig.

The insertion mechanism consists of a ladle or spoon with a small pipe running down the centre that has a capability to control the injection of air. The air is injected through this pipe into the upside-down ladle using a syringe. The cup will then need to be twisted to allow the bubble to rise.

The second rig was designed with acrylic tube of 400 mm in diameter and 2.0 m in height. Larger sizes of bubble were tested in this rig to eliminate the wall effect.

The camera lifting apparatus stands approximately 2.0 m high which allows the movement of the camera mount device to rise through 1.8 m in height. The variable speed drive of camera lifting apparatus regulates the control of the camera mount device. This drive allows the camera to be raised at approximately the same velocity as the bubble.

A high speed digital video camera was mounted on a device with a small attachment to the side of the camera lifting apparatus.

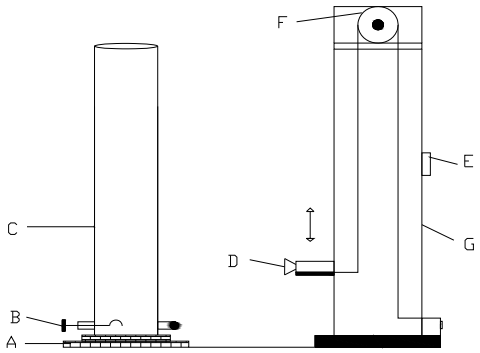


A = Sturdy Base; B = Rotating Spoon; C = Cylindrical test rig (0.125m or 0.40 m diameter), D = Video camera; E = Variable speed motor; F = Pulley; and G = Camera lifting apparatus.

**Fig. 1** Schematic diagram of experimental apparatus

### 2.2 Bubble rise velocity measurement

A known volume of air bubble was injected from injection apparatus close to the bottom of the test rig. The injection apparatus was designed in such a way that allows controllable quantities of air into the test rig. A high speed digital video camera was used to record the bubble motion as they rose through liquids. These bubble videos clips were analysed by 'Windows Movie Maker' where various bubble rise times were noted. Bubble rise velocities over these times were calculated since the distance travelled was known.

### 2.3 Bubble diameter measurement

Bubble equivalent diameter was measured from the still images which were obtained from the video clips. The still images were then opened using commercial software "SigmaScan Pro 5.0" and the bubble height ($d_h$) and the bubble width ($d_w$) were measured in pixels. The pixel measurements were converted to millimetres based on calibration data for the camera. The bubble equivalent diameter, $d_{eq}$ was calculated [22] as

$$d_{eq} = \left( d_h \times d_w^{\,2} \right)^{\frac{1}{3}} \quad (1)$$

### 2.4 Bubble trajectory measurement

Trajectory was determined from the still images collected from the digital video camera. Bubble trajectory was computed from the still frames obtained from the video image. The still frames were then opened in commercial software, "SigmaScan Pro"

which was capable of showing pixel location on an image.

The pixel coordinates (X and Y) of the bubbles centre were noted and recorded into spreadsheet. X coordinate corresponds to the distance from the left edge and Y coordinate corresponds to the distance from the top edge respectively. The pixel line running through the centre of the bubble release point was known. The deviation of the bubble centre from the release point was computed by subtracting the X of the bubble centre from the X of the bubble release point.

### 2.5 Calculation of Re and drag coefficient

The terminal velocity of the bubble changes with the change in shear rate as the fluid viscosity changes as a function of the shear rate. The average shear rate over the entire bubble surface is equivalent to $U_b/d_b$ so the apparent viscosity can be written [16, 23] as

$$\mu = K\left(U_b/d_b\right)^{n-1} \tag{2}$$

In the case of spherical bubble, the Re for non-Newtonian power law fluid was rearranged from equation (2) as

$$\mathrm{Re} = \frac{\rho_{liq} d_b^n U_b^{2-n}}{K} \tag{3}$$

For a non-spherical bubble with a vertical axis of symmetry, the Re was defined [12, 16, 23, 24] by

$$\mathrm{Re} = \frac{\rho_{liq} d_w^n U_b^{2-n}}{K} \tag{4}$$

The drag co-efficient for spherical bubble was calculated by

$$C_d = \frac{4gd_b\Delta\rho}{3\rho_{liq}U_b^2} \tag{5}$$

In the case of non-spherical bubble, the drag co-efficient was computed by

$$C_d = \frac{4gd_{eq}^3\Delta\rho}{3\rho_{liq}d_w^2U_b^2} \tag{6}$$

## 2.6 Test fluids

Three different concentrations of xanthan gum solutions used in this study were a non-Newtonian (shear thinning) fluid. Water and xanthan gum with different concentrations of 0.025%, 0.05% and 0.1% (by weight) were used. These non-Newtonian solutions were prepared by mixing xanthan gum by weight of each concentration with water in the test rig and stirring it for long hours (5-7 hrs). The temperature of water and all solutions in this study was maintained at $25^{\circ}C$. For every solution, the measured density was very close to the density of water at $25^0$ C since they were made with low concentrations of xanthan gum in the solution.

### 2.6.1 Fluid Characterization

The rheological properties of the solutions were measured using an ARES (Advanced Rheometric Expansion System) rheometer. The range of shear rates to determine fluid rheology was 1 $s^{-1}$ - 650 $s^{-1}$. The rheological properties for different concentration of xanthan gum solutions tested are illustrated in Fig. 2 and summarized in Table 1.

Figure 2 shows that the three different xanthan gum solutions exhibit non-Newtonian shear-thinning pseudoplastic behaviour which is adequately described by Power-Law model given below.

$$\eta = K\dot{\gamma}^{n-1} \tag{7}$$

The K and n values for the xanthan gum solutions were determined from this response curve and are shown in the Table 1.

**Table 1** Rheological and physical properties of xanthan gum solutions.

| Fluid Type | Concentration (%) | K, $Pa.s^n$ | n | Density, $kg/m^3$ |
|---|---|---|---|---|
| Xanthan gum | 0.025 | 0.00612 | 0.8248 | 996.0 |
| Xanthan gum | 0.05 | 0.03024 | 0.6328 | 996.0 |
| Xanthan gum | 0.1 | 0.09503 | 0.5481 | 997.0 |

K represents the consistency of the fluid behaviour i.e. the higher the value of K, the more viscous the fluid and n denotes power law index which is a measure of the extent of non-Newtonian behaviour. For shear-thinning pseudoplastic liquids, the power law index, n, lies between zero and unity with values further removed form unity demonstrating a more pronounced non-Newtonian behaviour. As seen, the viscosity of xanthan gum increases with the increase in liquid concentration. On the other hand, power law index decreases with the increase in liquid concentration.

The xanthan gum solution with 0.1% concentration has the highest viscosity and low power law index in comparison with other concentrations used in this study.

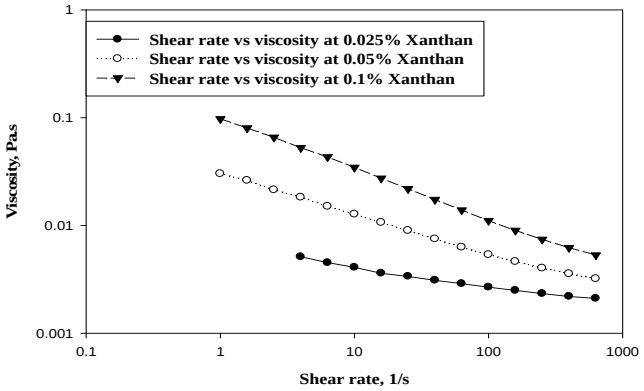


**Fig. 2** Viscosity vs. shear rate of xanthan gum solutions demonstrating the pseudoplastic behaviour.

# 3 Results and Discussion

## 3.1 Comparison between bubble rise velocity and bubble equivalent diameter

The current results of bubble rise velocity as a function of the bubble equivalent diameter was compared with the result of Haberman and Morton [25] and Zheng and Yappa [26], see Figure 3. Figure 3 indicates that an increase in rise velocity with the increase of bubble diameter. As seen, the current experimental data agree well with these published data.

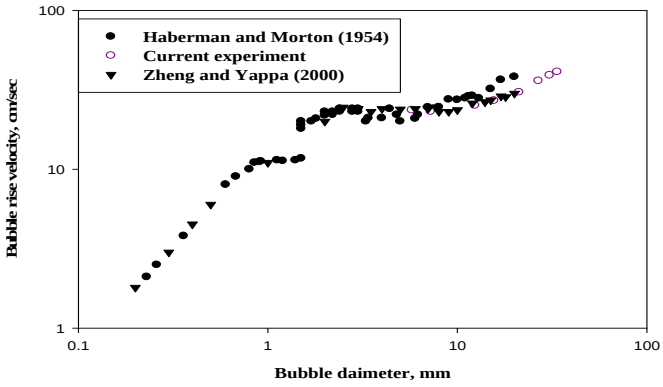


**Fig. 3** Bubble rise velocity vs. bubble equivalent diameter.

## 3.2 Bubble trajectory

The trajectory results of water are shown in Figure 4 for different bubble sizes when measured over a height of 1.0 m from the point of air injection and Fig. 5 displays the schematic pictures of the bubble trajectories of different sizes of air bubbles in water.

Figure 4 shows the deviation of bubble from its release point as it rises through water. The general trend was for the bubble to remain close to the release centre, when the bubble was released and as it rose through water, it spread out as the height increases.

For water, the smaller bubble (0.1mL) deviated more horizontally with respect to the bubble release centre and the bubble started to rise with helical or zigzag motion. It was seen that the path instability occurs from the equivalent diameter of 3.38 mm which equates to a Weber number 2.57. This phenomenon agrees well with the findings of Duineveld [27] and Leal [28].

With increasing bubble size, the bubble surface oscillations change from a simple oscillation to higher order modes, the trajectory changes from a simple helix to more complex trajectories. For larger bubbles, it was seen from Figure 4 and Figure 5 that initially, the bubble followed straight path, attained its terminal velocity and shape, then it switched to spiral path.

The larger bubble of 5.0mL, at high Re of 4331 and Weber number of 11.77, initially deviated horizontally with zigzag motion and it then, travelled in straight path and finally, followed a spiral path.

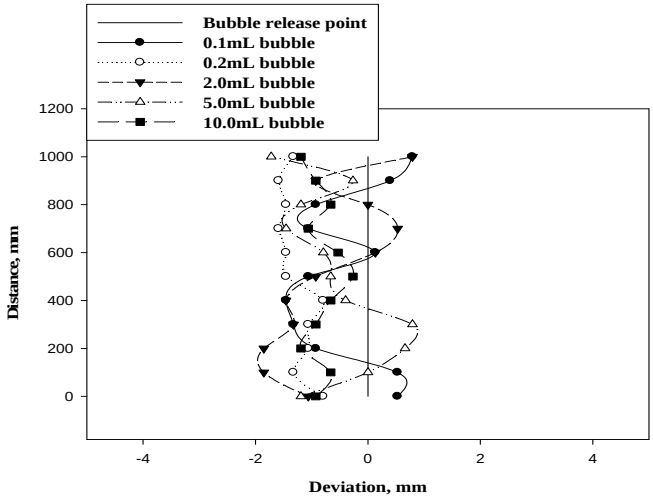


**Fig. 4** Rise trajectories of different sizes of bubbles in water.

The 10mL bubble, in the beginning, followed the straight path, and it then followed spiral path and finally, straight path until it finished its journey.

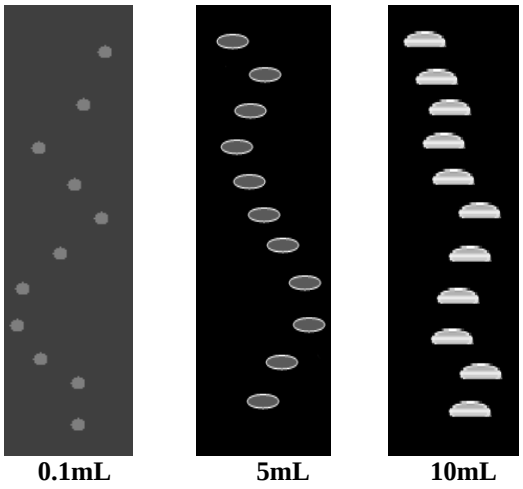


**Fig.5** Schematic rise trajectories of different sizes of air bubbles in water.

It was seen that the spiral motion never changed into the zigzag motion in this study that was also found by saffman [8] in the literature. Clift et al. [19] and Duineveld [27] investigated the smaller bubbles less than 2 mm in diameter rise in straight or linear path but the linear trajectory was not observed in this study as the bubble equivalent diameter of this study was more than 3 mm. For smaller bubble at low Reynolds number, the rising bubble showed a zigzag trajectory [5, 6, 29, 30]. The larger bubbles at high Reynolds number, displayed a spiral trajectory because the effect of wake shedding influenced the bubble to induce a spiraling rising motion.

The trajectory results of three different concentrations of xanthan gum solution are shown respectively in Figure 6, Figure 8 and Figure 9 for different bubble sizes. The schematic diagram of rise trajectories of 0.025% xanthan gum solution for different bubble volumes are shown in Figure 7. It is seen from Figure 6 and Figure 7, the horizontal deviation of the smaller bubble (0.1mL) is less than that of water. This is due to increased viscosity of the solution and less friction acting upon their surface compared to the larger bubbles and so the smaller bubbles experience less resistance to vertical movement.

The larger bubbles (5.0mL and 10mL) initially choose straight path and it then deviated horizontally and finally, they switched to a spiral path. But 10mL bubble exhibited more spiral motion than that by 5mL bubble. The larger bubbles however experience more resistance on top and deform as their size increases which results in spiral motion.

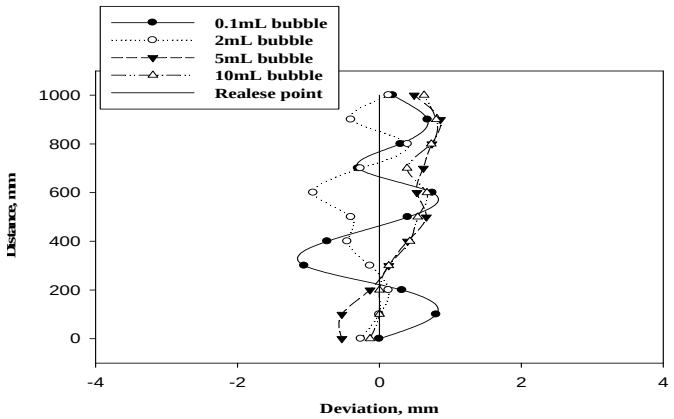


**Fig. 6** Rise trajectories of different sizes of bubbles in 0.025% xanthan gum solution.

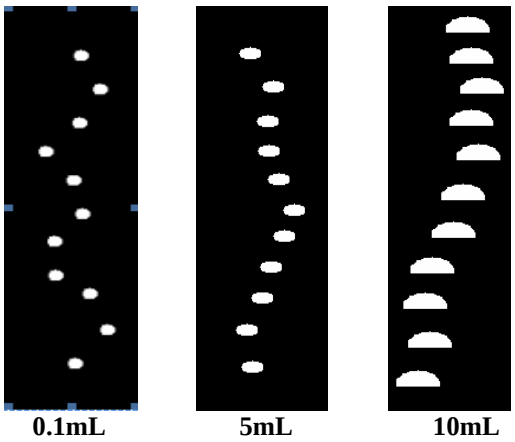


**Fig.7** Schematic rise trajectories of different sizes of air bubbles in 0.025% xanthan gum.

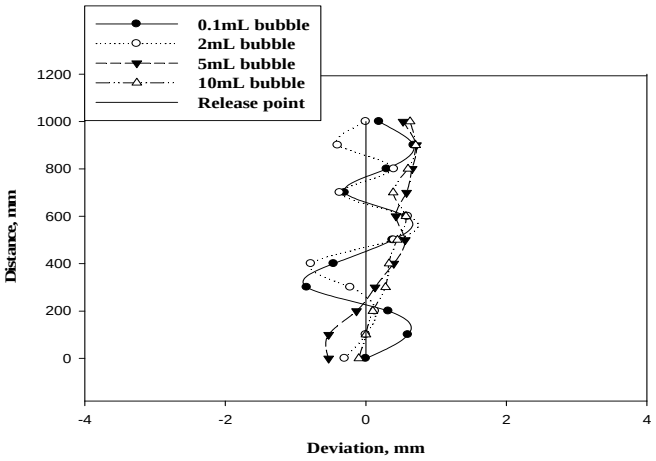


**Fig. 8** Rise trajectories of different sizes of bubbles in 0.05%% xanthan gum solution.

It is observed from Figure 8 and Figure 9 that the horizontal movement for smaller bubbles was less with the increase in xanthan gum concentration. Therefore, smaller bubble of high concentration (0.1%) xanthan gum solution exhibits a less horizontal deviation. On the other hand, larger bubbles of high concentration (0.1%) xanthan gum produced more spiral motion in comparison with other concentrations of xanthan gum used in this study.

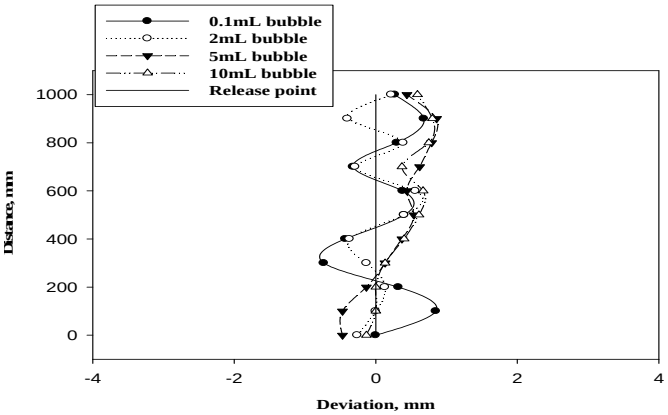


**Fig. 9** Rise trajectories of different sizes of bubbles in 0.1%% xanthan gum solution.

### 3.3 Drag co-efficient

Bubble drag coefficients as a function of Re for water are presented in Fig. 10. For $\mathrm{Re} \le 0.1$, the creeping flow regime, the well known Stokes model is given by

$$C_d = \frac{24}{\mathrm{Re}} \tag{8}$$

For low Re (<0.1), the bubble velocity is dependant on the viscosity of the fluid and the gas bubble follows Hadamard-Ryczynski model at very low Re rather than Stokes model due to the internal circulation of the gas bubble which is given [17] by

$$C_d = \frac{16}{\mathrm{Re}} \tag{9}$$

For any Re, the following equation (10) was suggested [31] for spherical bubble.

$$C_d = \frac{16}{\mathrm{Re}}\left\{1+\left[\frac{8}{\mathrm{Re}}+\frac{1}{2}\left(1+3.315\,\mathrm{Re}^{-0.5}\right)\right]^{-1}\right\} \tag{10}$$

As seen, the equations (8), (9) and (10) give a reasonable fit at high Re when the current experimental data were compared.

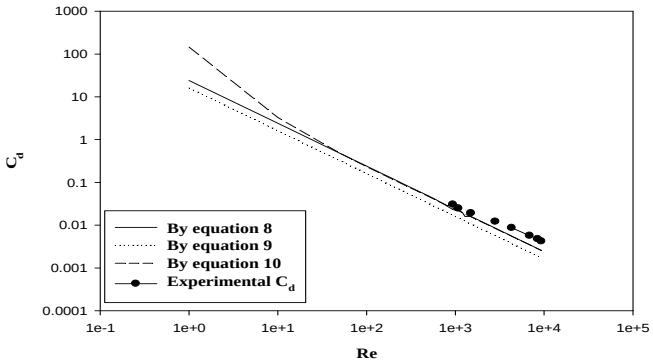


**Fig. 10** Drag coefficients vs. Reynolds number for rising air bubble in water.

Many authors have predicted the drag relationship which focused on either spherical bubble or solid particle. There have been limited studies available in the literature on drag co-efficient of spherical and non-spherical bubble at high Re in non-Newtonian power-law fluids.

The most widely accepted correlation of drag coefficient for solid particles was developed by Turton and Levenspiel [32] and is given by

$$C_d = \frac{24}{\mathrm{Re}}\left(1+0.173\,\mathrm{Re}^{0.657}\right)+\frac{0.413}{1+16{,}300\,\mathrm{Re}^{-1.09}} \tag{11}$$

The above correlation converges to Stokes model at low Re. A modified correlation proposed for gas bubbles in non-Newtonian power-law fluids [12], is given by

$$C_d = \frac{16}{\mathrm{Re}}\left(1+0.173\,\mathrm{Re}^{0.657}\right)+\frac{0.413}{1+16{,}300\,\mathrm{Re}^{-1.09}} \tag{12}$$

The equation (12) converges to the Hadamard - Rybczynski equation, at low Re.

The following equation (13) was also suggested for bubbles [33],

$$C_d = \left[2.25\,\mathrm{Re}^{-0.31}+0.36\,\mathrm{Re}^{0.06}\right]^{3.45} \tag{13}$$

The above equation (13) is valid for ($10^{-2}$< Re <$3*10^5$).

It is seen from Figure 10 that the experimental $C_d$ of 0.025% xanthan gum solution shows a good fit at higher Re in comparison with the equations (11), (12) and (13).The experimental $C_d$ in Fig.11 shows the exact match with the equation (13) when it was compared with the above mentioned equations. The same phenomenon is also observed in Fig.12 for 0.1% xanthan gum solution.

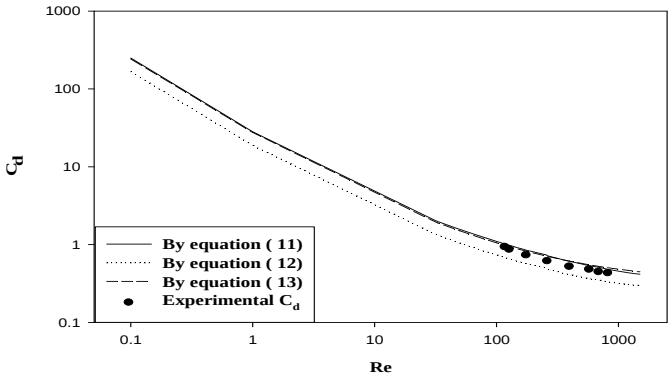


**Fig.10** Drag coefficients vs. Reynolds number for rising air bubble in 0.025% xanthan gum solution.

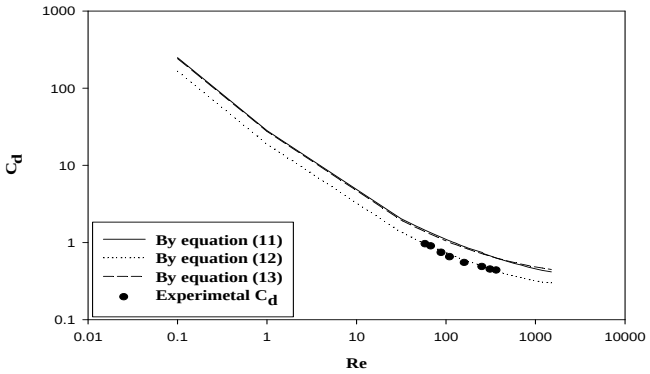


**Fig.11** Drag coefficients vs. Reynolds number for rising air bubble in 0.05% xanthan gum solution.

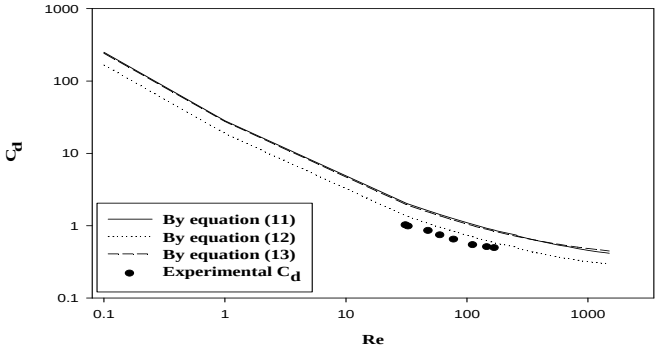


**Fig.12** Drag coefficients vs. Reynolds number for rising air bubble in 0.1% xanthan gum solution

The reported experimental data of drag coefficient increases with the increase in xanthan gum concentration for corresponding bubble volume. As seen, these new data are agreed well with the published equations mentioned above.

# 5 Conclusion

The bubble rise characteristics, namely, bubble velocity, trajectory and drag coefficient produced acceptable and consistent results.

The bubble equivalent diameter in water observed a reasonable fit with the published literature.

The trajectory analysis showed that small bubbles followed a helical or zigzag motion while larger bubbles followed a spiral motion for water.

For water, the horizontal motion observed was less when the bubble size increased.

In the case of xanthan gum solutions, the small bubbles experienced less horizontal motion than that of water. On the other hand, larger bubbles produced more spiral motion with the increase in xanthan gum concentration.

The experimental data of drag coefficient increases with the increase in xanthan gum concentration for corresponding bubble volume. The relationship between $C_d$-Re for different concentration xanthan gum solutions showed acceptable results with the available analytical and experimental studies in the literature with a wide range of Reynolds numbers.

*Nomenclature:*

| | | |
|---|---|---|
| $d_b$ | [m] | bubble characteristic diameter |
| $d_h$ | [m] | bubble height or short axis length |
| $d_w$ | [m] | projected diameter onto horizontal plane or long axis length |
| $d_{eq}$ | [m] | equivalent sphere diameter |
| $\mu$ | [Pa.s] | apparent viscosity |
| Re | [-] | Reynolds number |
| $C_d$ | [-] | drag coefficient |
| $F_d$ | [N] | drag force |
| $g$ | [m/s$^2$] | acceleration due to gravity |
| $U_b$ | [m/s] | bubble rise velocity |
| $n$ | [-] | power law index |
| $K$ | [Pa.s$^n$] | fluid consistency index |
| g | [m/s$^2$] | gravitational acceleration |

Greek letters

$\Delta\rho$ [kg/m$^3$] density difference between liquid and air bubble
$\rho_{liq}$ [kg/m$^3$] liquid density
$\dot{\gamma}$ [s$^{-1}$] shear rate
$\eta$ [Pa.s] non-Newtonian viscosity,

*Acknowledgments:*
The authors gratefully acknowledges the financial support from Sugar Research Institute, Queensland, Australia and the technical assistance provided by Mr. Ray Kerney in the experimental works. N.M.S. Hassan is thankful to Central Queensland University for the award of a research scholarship to pursue this study.

*References:*

[1] Shosho, C. and Ryan, Micheal, E., An experimental study of the motion of long bubbles in inclined tubes, Chemical engineering science, 56, 2001, 2191-2204.
[2] Kulkarni, A. A. and Joshi, J. B., Bubble Formation and Bubble Rise Velocity in Gas-Liquid Systems: A Review, Ind. Eng. Chem. Res., 44, 2005, 5873-5931.
[3] Shew, W. L., Poncet, S. and Pinton, J. F., Viscoelastic effects on the dynamics of a rising bubble, Journal of statistical Mechanics, P01009, 2006.
[4] Wu, Mingming. and Gharib, Morteza., Experimental Studies on the Shape and Path of Small Air Bubbles Rising in clean Water, Physics of Fluids, vol.14, no.7, 2002.
[5] Hassan, N. M. S., Khan, M. M. K., Rasul, M. G. and Rackemann, D.W., An Experimental Study of Bubble Rise Characteristics in non – Newtonian (Power-Law) Fluids, Proceedings of the 16th Australasian Fluid Mechanics Conference, Gold Coast, Australia, 2007,1315-1320.
[6] de Vries, A. W. G., Biesheuvel, A. and van Wijngaarden, L., Notes on the path and wake of a gas bubble rising in pure water, Int. J. Multiph. Flow 28, 1823, 2002.
[7] Mougin, G. and Magnaudet, J., Phys. Rev. Lett. 88, 014502, 2002.
[8] Saffman, P.G., On the rise of small air bubbles in water. Journal of Fluid Mechanics, Digital Archive, 1956, 1: 249-275, Cambridge University Press.
[9] Feng, Z. C. and Leal, L.G., Nonlinear bubble dynamics, Annu. Rev. Fluid mech., 29, 1997, 201.
[10] Yoshida, S. and Manasseh, R., Trajectories of rising bubbles, the 16th Japanese Multiphase Flow Symposium, Touha, Hokkaido, July, 1997.
[11] Shew, W. L. and Pinton, J. F., Dynamical Model of Bubble path Instability, PRL 97, 144508, 2006
[12] Dewsbury, K., Karamanev, D. G. and Margaritis, A., Hydrodynamic Characteristics of free Rise of Light solid Particles and Gas Bubbles in Non-Newtonian Liquids, Chemical engineering Science, vol. 54, 1999, 4825-4830.
[13] Tsuge, H., and Hibino, S., The motion of Single Gas Bubbles Rising in Various Liquids, Kagaku Kogaku, 35, 65, 1971.
[14] Dewsbury, K., Karamanev, D .G. and Margaritis, A., Dynamic Behavior of Freely Rising Buoyant Solid Spheres in Non-Newtonian Liquids, AIChE Journal, Vol. 46, No. 1, 2000.
[15] Dewsbury, K., Karamanev, D. G. and Margaritis, A., Rising solid sphere hydrodynamics at high Reynolds numbers in non-Newtonian fluids, Chemical Engineering Journal, 87, 2002, 129-133.
[16] Margaritis A., te Bokkel, D. W. and Karamanev, D. G., Bubble Rise Velocities and Drag Coefficients in non-Newtonian Polysaccharide solutions, John Wiley & Sons, Inc., 1999.
[17] Miyahara, T. and Yamanaka, S., Mechanics of Motion and Deformation of a single Bubble Rising through Quiescent Highly Viscous Newtonian and non-Newtonian Media, Journal of chemical engineering, Japan, Vol. 26, No. 3, 1993.
[18] Dhole, S. D., Chhabra, R. P. and Eswaran, V., Drag of a Spherical Bubble Rising in Power Law Fluids at Intermediate Reynolds Numbers, Ind. Eng. Chem. Res. 46, 2007, 939 – 946.
[19] Clift, R., Grace, J. R and Weber, M. E., Bubbles, Drops and Particles; Academic Press, 1978, republished by Dover, 2005.
[20] Chhabra, R. P., Bubbles, Drops, and Particles in Non-Newtonian Fluids, Taylor & Francis Group CRC Press, 2006.
[21] Karamanev, D. G., Rise of gas Bubbles in Quiescent Liquids, AIChE Journal, Vol. 40, 1994, No.8.
[22] Lima-Ochoterena, R. and Zenit, Visualization of the flow around a bubble moving in a low

viscosity liquid, Revista Mexicana De Fisica 49 (4), 2003, 348 – 352.

[23] Lali, A. M., Khare, A. S., Joshi, J. B. and Nigam, K. D. P., Behaviour of Solid Particles in viscous Non-Newtonian Solutions: Settling Velocity, Wall Effects and Bed Expansion in Solid-Liquid Fluidized Beds, Powder Technology, 57, 1989, 39 – 50.

[24] Miyhara, T. and Takahashi, T., Drag coefficient of a single bubble rising through a quiescent liquid., International Chemical Engineering, Vol. 25, No. 1, 1985.

[25] Haberman, W. L. and Morton, R. K., An Experimental Study of Bubbles moving in Liquids, *ASCE*, 387, 1954, pp.227-252.

[26] Zheng, Li and Yapa, P.D., Buoyant Velocity of Spherical and Non spherical Bubbles/Droplets, Journal of Hydraulic Engineering, Vol. 126, No. 11, 2000.

[27] Duineveld, P. C., The Rise Velocity and Shape of Bubbles in pure water at high Reynolds Number, J. Fluid Mech. vol. 292, 1995, 325-332.

[28] Leal, L. G., Velocity transport and wake structure for bluff bodies at finite Reynolds number, Physc. Fluids A 1, 1989, 124-131.

[29] N. M. S. Hassan, M. M. K. Khan and M. G. Rasul, Characteristics of air Bubble Rising in Low Concentration Polymer Solutions, WSEAS TRANSACTIONS on FLUID Mechanics, ISSN: 1790-5087, Issue 3, Vol. 2, 2007.

[30] Krishna, R., van Baten, J.M., Rise Characteristics of Gas Bubbles in a 2D Rectangular Column: VOF Simulations vs. Experiments, Int. Comm. Heat Mass Transfer, vol. 26, no. 7, 1999, 965-974.

[31] Mei, R. and Klausner, J. F., Unsteady force on a spherical bubble at finite Re with small functions in the free stream velocity, Phys. Fluids. A, 4, 1992, 63.

[32] Turton, R., and Levenspiel, O., A short note on the drag correlation for spheres, Powder Technology, 4, 1986.

[33] Khan. A. R. and Richardson, J. F., The resistance to motion of a solid sphere in a fluid, Chem. Eng. Comm., vol. 62, 1987, 135 – 150.